UNIVERSITY OF BIRMINGHAM

University of Birmingham Research at Birmingham

Thermal management performances of PCM/water cooling-plate using for lithium-ion battery module based on non-uniform internal heat source

Bai, Fanfei; Chen, Mingbiao; Song, Wenji; Feng, Ziping; Li, Yongliang; Ding, Yulong

[Link to publication on Research at Birmingham portal](#)

Accepted Manuscript

Research Paper

Thermal management performances of PCM/Water cooling-plate using for lithium-ion battery module based on non-uniform internal heat source

Fanfei Bai, Mingbiao Chen, Wenji Song, Ziping Feng, Yongliang Li, Yulong Ding

Please cite this article as: F. Bai, M. Chen, W. Song, Z. Feng, Y. Li, Y. Ding, Thermal management performances of PCM/Water cooling-plate using for lithium-ion battery module based on non-uniform internal heat source, *Applied Thermal Engineering* (2017), doi: http://dx.doi.org/10.1016/j.applthermaleng.2017.07.141

Thermal management performances of PCM/Water cooling-plate using for lithium-ion battery module based on non-uniform internal heat source

Fanfei Bai,[a,b,c,d]   Mingbiao Chen,[a,b,c]   Wenji Song,[a,b,c]*   Ziping Feng[a,b,c] ,   Yongliang Li,[e]   Yulong Ding,[e]

[a]Guangzhou Institute of Energy Conversion, Chinese Academy of Sciences, Guangzhou 510640, China

[b]CAS Key Laboratory of Renewable Energy, Chinese Academy of Sciences, Guangzhou 510640, China

[c]Guangdong Provincial Key Laboratory of New and Renewable Energy Research and Development, Guangzhou 510640, China

[d]University of Chinese Academy of Sciences, Beijing 10049, China

[e]School of Chemical Engineering, University of Birmingham, Birmingham B152TT, United Kingdom

The following is the e-mail of authors.:

1) Name: Fanfei Bai   E-mail: baiff@ms.giec.ac.cn

2) Name: Mingbiao Chen   E-mail: chenmb@ms.giec.ac.cn

3) Name: Wenji Song*   E-mail: songwj@ms.giec.ac.cn

4) Name: Ziping Feng   E-mail: fengzp@ms.giec.ac.cn

5) Name: Yongliang Li   E-mail: y.li.1@bham.ac.uk

6) Name: Yulong Ding   E-mail: Y.Ding@bham.ac.uk

Highlight:

The lithium battery module with Phase change material/water cooling-plate was proposed.

The non-uniform internal heat source based on 2D electro-thermal model for battery LiFePO4/C was used.

The water cooling-plate can cool the high heat generation area of battery effectively.

The Phase change material /water cooling plate can prevent the thermal runaway at the end of 5 continuous

charge-discharge cycles.

Abstract: In order to improve the working performance of the lithium-ion battery, the battery module with Phase

change material/water cooling-plate was designed and numerically analyzed based on the energy conservation and

fluid dynamics. The non-uniform internal heat source based on 2D electro-thermal model for battery LiFePO4/C

was used to simulate the heat generation of each battery. Then factors such as height of water cooling-plate, space

between adjacent batteries, inlet mass flow rate, flow direction, thermal conductivity and melting point of PCM

were discussed to research their influences on the cooling performance of module. And the 5 continuous

charge-discharge cycles was used to research the effect of PCM/water cooling plate on preventing thermal runaway.

The results showed that the water cooling plate set close to the near-electrode area of battery removed the majority

of heat generated during discharging and decreased the maximum temperature efficiently. The PCM between the

adjacent batteries could improve the uniformity of temperature field. In addition, the PCM/water cooling plate

could limit the maximum temperature effectively and improve the uniformity of temperature field during the 5

continuous charge-discharge cycles. As a result, it prevented the emergence of thermal runaway and increased the

safety of module.

Nomenclature

T_{Max} the maximum temperature (K)

T_{Min} the minimum temperature (K)

ΔT maximum temperature difference (K)

c specific heat ($J \cdot kg^{-1} \cdot K^{-1}$)

A area (m^2)

Q mass flow rate ($kg \cdot s^{-1}$)

q heat (J)

L latent heat ($J \cdot kg^{-1}$)

T_0 ambient temperature (K)

P static pressure (Pa)

R   resistances (Ω)

H enthalpy ($J \cdot kg^{-1}$)

ΔG gibbs free energy change ($J \cdot kg^{-1}$)

ΔS entropy change ($J \cdot kg^{-1} \cdot K^{-1}$)

h convective heat transfer coefficient ($W \cdot m^{-2} \cdot K^{-1}$)

Nu Nusselt number

Gr Grashof number

Pr Prandtl number

α_V coefficient of cubical expansion

g gravitational acceleration

Greek symbols

υ viscosity ($kg \cdot m^{-1} \cdot s^{-1}$)

$\vec{\upsilon}$ velocity vector

ρ density ($kg \cdot m^{-3}$)

λ thermal conductivity ($W \cdot m^{-1} \cdot K^{-1}$)

τ time constant

Subscripts

b battery

w water

aver   average

out   outlet

in   inlet

Al aluminum

Max   maximum

X   X direction

Y   Y direction

Z   Z direction

j   joule

r   reversible

p   irreversible

m   arithmetic mean

Acronyms

PCM   phase change material   SOC   state of charge

BTM   battery thermal management

1. Introduction

Because of the property of high specific power, high specific energy density, long cycle life, low self-discharge rate and high discharge voltage, the lithium-ion batteries have been widely used in developing the clean energy transportation and had become a prime power source solution for battery electric vehicles and hybrid electric vehicles [1]. During charging and discharging cycles the lithium-ion batteries will be overheated due to the heat generation which cannot be dissipated to the environment timely. And the performances, safety and service life will all be greatly affected [2]. As the large-scale battery packs are consist of many cells connected in series or parallel, the maximum temperature difference between cells in a module may lead to a premature failure of the whole pack [3]. Battery thermal management (BTM) system is therefore required to help the battery operate at a desirable working temperature at all times. The BTM system includes air cooling system, phase change material (PCM) based cooling system and liquid cooling system. As different part of pouch lithium-ion battery has different heat generation during the discharging, the non-uniformity of the temperature distribution increase with time, especially in the large capacity battery [4]. The BTM system combining different cooling manners makes better cooling performance, compared with the BTM system with single cooling manner [5].

As the PCM has a large latent heat and appropriate melting point, it can store/release large amounts of heat during the melting/solidifying process. So the PCM is used in the BTM system to give rise to a relatively constant temperature of the battery system. The heat generated by the battery was absorbed by PCM and then removed by the ambient air which is contact with the battery case. PCM eliminates the need for active cooling/heating during the majority of operating time because it delays the temperature rise when the ambient is cold and maintains the

4

battery below ambient during hot days[6]. The wax was used as the PCM, as first proposed by Al-Hallaj and Selman

[7,8].The effects of PCM on square lithium-ion battery was investigated and the results indicated that PCM could

improve the uniformity of temperature distribution and keep battery in safe temperature range[9]. Kizilel et al.

investigated small format cells surrounded by a wax composite material of expanded graphite and wax and they

pointed that the latent heat of the wax could help prevent a propagating failure [10]. Unfortunately, one of the most

important bottlenecks that limit the applications of PCM on BTM system is that the thermal conductivity is poor.

This can lead to big thermal gradient of the battery pack. So many approaches were used to solve the conflict

between large heat storage capacity and low thermal conductivity. Such as, combining the PCM with porous

materials [11]; adding high thermal conductivity substances in paraffin [12]; developing PCM based BTM system

with metal finned structure [13]; and add a metal matrix into PCM. However, the thermal conductivity increases at

the cost of decreasing latent heat, which determined storage capacity. The appropriate ratio of thermal conductivity

between PCM and battery is necessary, so as to achieve a good cooling performance and decrease the mass and

volume. W.Q. Li et al. [14] designed a sandwiched cooling structure using copper metal form saturated with PCM.

The composited PCM presented a much better cooling effect compared to pure PCM. Rao investigated the effect of

PCM phase change temperature on thermal management. They pointed out that if the melting point is below 318.15

K, it will be conductive to heat diffusion [15].Jiang et al. [16] fount that the PCM-based BTM system showed better

performance than the forced convection BTM system under the same condition and the PCM was able to control

the temperature of the pack during the melting process.

Compared with other PCM, liquid has higher thermal conductivity which leads to higher cooling performance

and is more suitable for large-scale battery pack. Liquid cooling can well decrease the maximum temperature and

the maximum temperature difference during the charging and discharging process. Nelson et al. [17] compared

different cooling system for lithium-ion batteries. The results showed that the liquid cooling effect was more

effective than other cooling manner. Higher heat transfer coefficient of water enables cold-plate to effectively

remove a large amount of heat from the batteries in the liquid cooling system. Chen et al. [18] found that an indirect

liquid cooling system had the lowest maximum temperature rise, and was more practical than direct liquid cooling.

Zhao et al. [19] designed a mini-channel liquid cooled cylinder to cool the cylindrical battery. The results showed

that the maximum temperature was no more than 40 ℃, as the number of mini-channel was no less than four and

the inlet mass flow rate was 1×10^{-3} kgs^{-1}. An oblique liquid cold plate was designed by Jin et al. [20] The results

showed that the oblique mini-channel could get higher heat transfer coefficient than conventional straight

mini-channel. Huo et al. [21] designed a mini-channel cold-plate based BTM system. The results showed that the

maximum temperature of pack decreased with the increase of the channel number and inlet mass flow rate. Panchal

et al. [22] designed and optimized the battery systems with mini-channel cold plates placed on the prismatic

lithium-ion battery cell. The experiment and simulation result showed that the cold plates displayed a good cooling

performance. Zhen et al. [23] concluded that the mini-channel cold-plate BTM system provided good cooling

efficiency in controlling the battery temperature at 5C discharging. A 5-channel cold-plate was enough and the

temperature could be evidently reduced by increasing the inlet mass flow rate. Panchal et al. [24] used cold plate

approach with the indirect liquid cooling method to cool the pouch lithium-ion battery at 1 C, 2 C, 3 C and 4 C

discharging rates and different environment temperature. Liu et al. [25] researched the thermal behaviors in

lithium-ion batteries. The results showed that different cooling methods should be adopted under different ambient

temperature conditions. They concluded that the liquid cooling made the strongest cooling effect under a normal

environment temperature condition and the Reynolds number influenced the effect of the liquid cooling

performance greatly.

Rao et al.[26] investigated the thermal performance of PCM/mini-channel coupled BTM system. The

mini-channel was set in the PCM to remove the heat and prevent the PCM lose efficacy. The maximum

6

temperature could be reduced 14.8 K and this system presented more effective thermal performance and compared with the PCM based system. In their simulation the heat source of battery was uniform. Actually, the heat generation of different parts in battery is different. Such as the heat generation rate of near-electrode area was high. And the temperature of near-electrode area of the battery was higher than other region, which made the non-uniformity of temperature. It is obvious that the difference about battery heat generation was not considered in their research. The employing of uniform heat source can lead to big error.

In conclusion, liquid cooling method can achieve the good cooling effect and PCM cooling method can acquire the most uniform temperature distribution. Considering the large heat storage capacity of the PCM and the excellent cooling effect of liquid cooling, we combined the PCM and the liquid cooling system to optimize the temperature field of lithium-ion battery module. The water cooling-plate was used to cool the near-electrode area with high heat generation rate. And the PCM was used to absorb the heat generated by other parts of battery. A 2-D heat source based on electro-thermal model was used to simulate the heat generation of pouch battery. The lithium-ion battery module with PCM/water cooling-plate was proposed and a three-dimensional thermal model was simulated. In this study, different influencing factors such as the height size of cooling plate, space between adjacent batteries, mass flow rate, flow direction, thermal conductivity and melting point of PCM were discussed in detail. And the 5 continuous charge-discharge cycles was used to research the effect of PCM/water cooling plate on preventing thermal runaway. The object of this study aimed to provide guidance for the thermal structure design of the lithium-ion battery module.

2. Model

2.1 Physical problem

The schematic of the module was shown clearly in Fig. 1. It can be seen that the PCM and the water

cooling-plate were filled into the gaps between the adjacent pouch batteries. The cooling plate was hollow and

filled with liquid water. The battery, PCM and water cooling-plate were packed in the module shell. As the model

was symmetrical, only 1/2 part of the module was simulated in this paper to shorten the simulation time. Heat

generated from the battery transferred into the water cooling-plate and PCM through contact surface. Water

removed the heat which was absorbed by the cooling plate. Inlet and outlet distributed on different sides of the

cooling plate. Considering higher temperature in the near-electrode area and better cooling performance of cooling

water, the cooling plate was set above the PCM. The thickness of the PCM and the water cooling-plate was equal to

the space between adjacent batteries. The shell of cooling-plate was made of aluminum due to its high thermal

conductivity and light weight. The thickness of aluminum was 0.5 mm. The physical sizes and thermal properties

of the battery, PCM, aluminum used in this paper are summarized in Table 1.
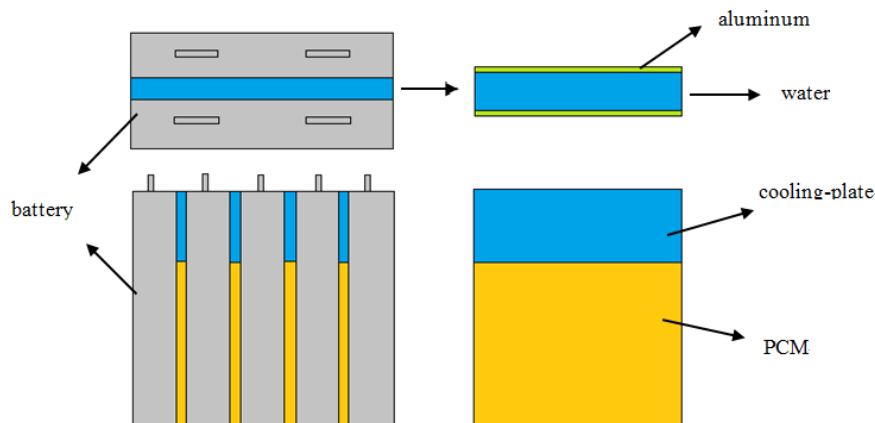
Fig. 1. Schematic of lithium-ion battery module with PCM/water cooling-plate

The battery was discharged at rate of 2 C to study the performance and the discharging could last for 1800 s.

Considering heat generation is not uniform in the actual battery, non-uniform heat source based on electro-thermal

model was used. The cooling water was assumed to be incompressible and laminar because the maximum Reynolds

number was less than 2300 in this study. The inlet water temperature, the initial temperature of batteries and PCM,

8

surrounding temperature were all equal which was set as 300 K. It is assumed that the properties of the PCM were

constant and equal for both solid and liquid phases [27].

Table 1 Physical sizes and parameters used in simulation

Nomenclature	Parameters	Value
Sizes of battery	(mm)	170×230×12
Capacity of battery	- (Ah)	40
Specific heat of battery	c_b (J·kg^{-1}·K^{-1})	2,138
Density of battery	ρ_b (kg·m^{-3})	1991
Thermal conductivity of battery in X-direction	λ_{b-X} (W·m^{-1}·K^{-1})	0.34
Thermal conductivity of battery in Y/ Z-direction	$\lambda_{b-Y/Z}$ (W·m^{-1}·K^{-1})	12
Cathode material of battery	-	Li_xC_6
Anode material of battery	-	$LiFePo_4$
Electrolyte of battery	-	$LiPF_6$
Specific heat of PCM	c_{PCM} (J·kg^{-1}·K^{-1})	2,000
Latent heat of PCM	L_{PCM} (J·kg^{-1})	247,000
Thermal conductivity of PCM	λ_{PCM} (W·m^{-1}·K^{-1})	0.151
Density of PCM	ρ_{PCM} (kg·m^{-3})	778
Viscosity of PCM	υ_{PCM} (kg·m^{-1}·s^{-1})	0.01
Specific heat of water	c_w (J·kg^{-1}·K^{-1})	4,182
Thermal conductivity of water	λ_w (W·m^{-1}·K^{-1})	0.6
Density of water	ρ_w (kg·m^{-3})	998.2
Viscosity of water	υ_w (kg·m^{-1}·s^{-1})	0.001003
Thermal conductivity of aluminum	λ_{Al} (W·m^{-1}·K^{-1})	202.4
Specific heat of aluminum	c_{Al} (J·kg^{-1}·K^{-1})	871
Density of aluminum	ρ_{Al} (kg·m^{-3})	2719
Ambient temperature	T_0 (K)	300

2.2 Governing equations

For a pouch battery, the heat transfer should follow the energy conservation law:

$$\rho_b c_b \frac{\partial T}{\partial t} = \lambda_b \nabla^2 T + q_{gen} \tag{1}$$

where ρ_b is density, λ_b is thermal conductivity, T is temperature, t is time and q is heat source. q_{gen} is the heat

generations of battery. The heat generation is included:

$$q_{gen} = q_j + q_p + q_r \tag{2}$$

where q_j is joule heat, q_p is irreversible electrochemical reaction heat and q_r is the reversible entropic heat.

9
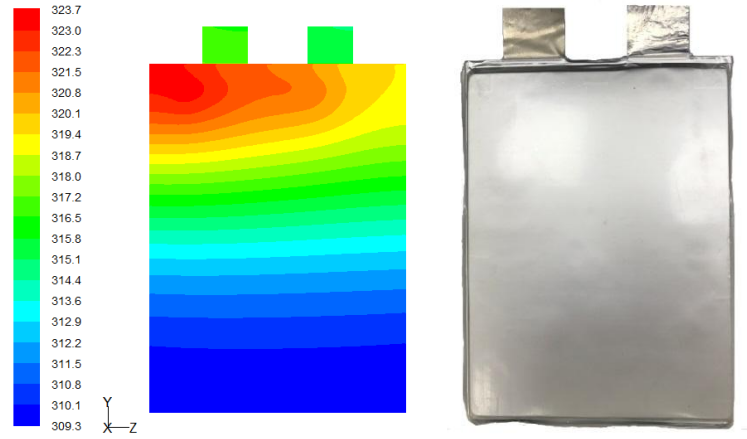
Fig. 2. Simulated temperature cloud of pouch battery at the end of 2 C discharging (left) and actual picture of the battery cell (right)

In our previous work, we had developed an electro-thermal coupled model for pouch battery LiFePO4/C in normal discharging progress [28]. Non-uniformity of temperature distribution was simulated and the result was validated with experiment data. The non-uniform internal heat source based on 2D electro-thermal model was got and the simulated temperature cloud of pouch battery at the end of 2 C discharging was shown in Fig. 2.

In the lithium-ion battery module, the heat generated in battery is absorbed by the PCM and removed by the cooling water, and then is taken away by the air.

The mass of the PCM can be derived by the equation as follows:

$$q_{pcm} = mc_{pcm}\left(T_1 - T_2\right) + mL \tag{12}$$

where T_1 and T_2 are the melting point and the initial temperature of PCM, respectively. q_{pcm} represents the heat absorbed by the PCM and c_{pcm} and L are specific heat and pure solvent melting heat of PCM, respectively.

The heat taken away by the cooling water is given as the following equation:

$$q_w = cm\Delta T = c_w \rho_w \mu_w A_{in}\left(T_{out} + T_{in}\right) \tag{13}$$

$$T_{aver} = \left(\frac{T_{out} + T_{in}}{2}\right) \tag{14}$$

Here, Q_w is the heat absorbed by water and T_{in} and T_{out} are the inlet and output temperatures of water, respectively.

A_{in} is the inlet area of water in the cooling plate. T_{aver} determined by T_{in} and T_{out}, is the average temperature of the

water. μ_w is the flow velocity of water. The values of ρ_w and c_w are the density and specific heat of water at T_{aver}.

According to Newton's law of cooling, the boundary equations in each direction can be expressed as follows:

$$-\lambda \frac{\partial T}{\partial x} = h(T - T_0), \quad x=0, \ X \tag{15}$$

$$-\lambda \frac{\partial T}{\partial y} = h(T - T_0), \quad y=0, \ Y \tag{16}$$

$$-\lambda \frac{\partial T}{\partial y} = h(T - T_0), \quad z=0, \ Z \tag{17}$$

Where T_0 is the ambient temperature. X, Y and Z respectively denote the size of the module in different direction.

The λ is thermal conductivity of module shell, which is made by aluminum. h is the convective heat transfer

coefficient that can be estimated as the following equation:

$$Nu_m = C(Gr \Pr)^n_m \tag{18}$$

$$Gr = \frac{g \alpha_V \Delta t l^3}{\upsilon^2} \tag{19}$$

$$h = Nu \frac{\lambda_{air}}{l} \tag{20}$$

$$Nu_m = 0.59(Gr \Pr)^{0.25}_m, \quad 1.43 \times 10^4 \le Gr \le 3 \times 10^9 \tag{21}$$

Where Nu_m is the Nusselt number, whose qualitative temperature is the arithmetic mean temperature of the boundary layer. Gr is Grashof number and the Δt is the difference of suface temperature and environment temperature. As the air is treat as ideal gas, the coefficient of cubical expansion α_V is equal to $1/T$ and the T is the arithmetic mean temperature of the boundary layer. l is the characteristic length and g is the gravitational acceleration. υ is the viscosity of air and λ_{air} is the thermal conductivity of air. Pr is the Prandtl number.

When the temperature of module shell is between 303 K and 313 K, the convective heat transfer coefficient is between 2.5 W·m^{-2}·K^{-1} and 3.7 W·m^{-2}·K^{-1}. In order to simplify the calculation, h is chose as 3 W·m^{-2}·K^{-1}. And the

error caused by *h* can be neglected.

The radiant heat transfer was not taken into account, as it was negligible.

As mentioned above, the PCM was used to absorb the heat generated by the low temperature area. As a part of PCM melt, the natural convection caused by gravity in the PCM during the melting process was less obvious. What's more, it has been calculated that there is little difference in the temperature field, comparing the model without the gravity and the model deal with the gravity. Therefore, the effect of the gravity was neglected and it is a problem of pure heat conduction during the melting process of PCM. The energy conservation equation in PCM can be seen as the following equation:

$$\rho \frac{\partial H}{\partial t} = \lambda \left(\frac{\partial^2 H}{\partial x^2} + \frac{\partial^2 H}{\partial y^2} + \frac{\partial^2 H}{\partial z^2} \right) \tag{22}$$

where ρ, H and λ are the density, enthalpy and thermal conductivity of PCM.

The water was selected as the cooling medium in the lithium-ion battery module. The energy conservation equation of liquid water within the cooling-plate is as follows:

$$\frac{\partial}{\partial \tau} \left(\rho_w c_w T_w \right) + \nabla \cdot \left(\rho_w c_w \vec{\upsilon} T_w \right) = -\nabla \cdot \left(\lambda_w \nabla T_w \right) \tag{23}$$

The momentum conservation equation of cooling water is given as follows:

$$\frac{\partial}{\partial \tau} \left(\rho_w \vec{\upsilon} \right) + \nabla \cdot \left(\rho_w \vec{\upsilon} \vec{\upsilon} \right) = -\nabla P \tag{24}$$

The continuity equation of the cooling water in the cooling plate is derived from follows:

$$\frac{\partial \rho_w}{\partial \tau} + \nabla \cdot \left(\rho_w \vec{\upsilon} \right) = 0 \tag{25}$$

where ρ_w and c_w are density and specific heat of liquid water, respectively. T_w represents the temperature of the water, $\vec{\upsilon}$ represents the velocity vector of water in cooling plate, and P is the static pressure.

3 Results and discussion

The height size of cooling plate, space between adjacent batteries, mass flow rate, and flow direction in water cooling-plate have significant effects on the cooling performance. So these four variables were studied. Besides, the effect of thermal conductivity and the melting point of PCM were simulated. The cooling performance was depicted by maximum temperature and maximum temperature difference which represented temperature uniformity. And the pressure drop of different signs was calculated, which indicated the energy consumption. At last the 5 continuous charge-discharge cycles was used to research the effect of PCM/water cooling plate on preventing the emergence of thermal runaway.

3.1 Effect of height of cooling plate

The height of cooling plate was changed from 2 cm to 7 cm in this section. The inlet mass flow rate was set as 1×10^{-3} kg·s^{-1}. The space of adjacent batteries was 4 mm. Fig. 3 (a) shows the maximum temperature, minimum temperature and maximum temperature difference in the pack under different height of cooling plate at the end of 2 C discharging. It can be seen that the maximum temperature of the pack increased firstly then decreased to minimum value and increased again to a relative stability index taking a "saddle pattern" when the height of cooling plate increased from 2 cm to 7 cm. When the height was 5 cm, the maximum temperature was 312.36 K. The minimum temperature of the module was almost unchanged and the variation trend of maximum temperature difference was the same with that of maximum temperature. As the height of cooling plate increased from 2 cm to 3 cm, the cross-sectional flow area of cooling water increased and the velocity of water decreased with the same mass flow rate. As a result, the coefficient of heat transfer decreased. And that would lead to the increase of maximum temperature. In this progress, the velocity of water played a leading role. As the height of cooling plate increased from 3 cm to 5 cm, the velocity of water and the coefficient of heat transfer reduced but the water-cooling area was

enlarged. The thermal heat dissipation was improved and the maximum temperature decreased. In this progress, the water-cooling area played a leading role. As the height of cooling plate increased to 7 cm continually, the cooling performance of high heat generation area decreased, which made the maximum temperature recover. The Fig. 3 (b) shows the temperature profile along the center line of cell and PCM close to the battery with different cooling plate height size at the end of 2 C discharging, as well as the temperature of center line of battery interior. It indicated that cooling plate with 5 cm in height performed better on improving the temperature uniformity along Y direction.
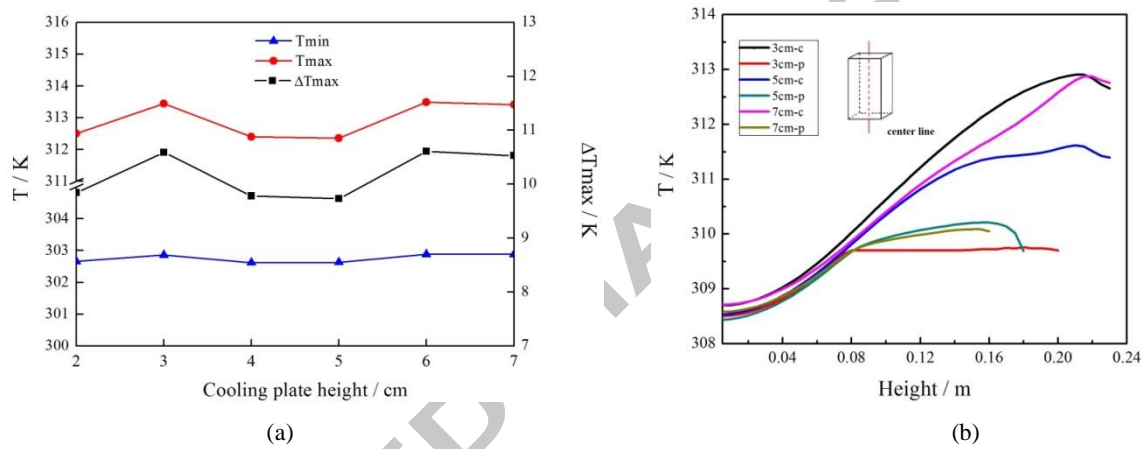
(a)   (b)

Fig. 3. (a) Temperature of the module under different cooling plate height. (b) Temperature of cell and PCM along the center line with different cooling plate height

The pressure drop is shown in Table 2. The result indicates that the pressure drop was affected obviously by the height size of cooling plate. When height size of cooling plate changed from 2 cm to 7 cm, pressure drop decreased 49.5%. As the height of cooling plate increased, the velocity of water in the plate decreased. And the frictional resistance decreased, which reduced the pressure drop of each cooling plates and energy consumption. But the downtrend of pressure drop was decelerated, when the height of cooling plate exceeded 5 cm.

Table 2 Pressure drop under different cooling plate height

Cooling plate height (mm)	2	3	4	5	6	7
Pressure drop (Pa)	27.9	20.7	17.4	15.8	14.7	14.1

The cooling performance was good as the height of cooling plate is 4 cm or 5 cm. Increase of the height led to increase of weight but lower pressure drop. Taking the above three factors into consideration, a 5 cm cooling plate in height is enough. So, in the following study, the 5cm high cooling plate was chosen.

3.2 Effect of space between adjacent batteries
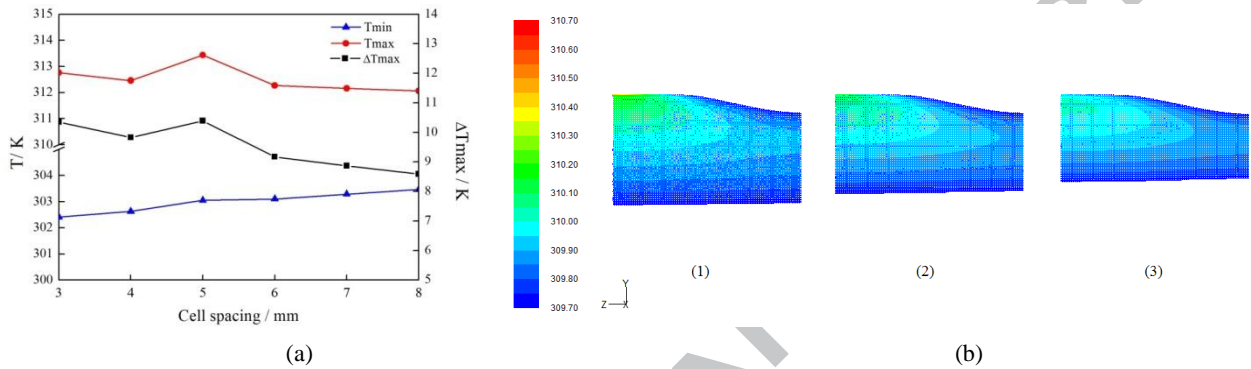
Fig. 4. (a) Temperature of the module under different space between adjacent batteries. (b) The PCM exceeded melting point closed to the battery with different space between adjacent batteries (4 mm, 6 mm, 8 mm)

The PCM and cooling plate was set between adjacent batteries, whose thickness was decided by the space between adjacent batteries. In this section the space between adjacent batteries was changed from 3 mm to 8 mm. The inlet mass flow rate was set as $0.001 \ kg \cdot s^{-1}$ and the height of cooling plate was 5 cm. Fig. 4 (a) shows that the maximum temperature decreased and minimum temperature increased as the space between adjacent batteries was changed from 3 mm to 8 mm. In addition, the uniformity of temperature field was improved obviously. When the thickness of the cooling plate increased, the cross-sectional flow area of cooling water was increased and the velocity of inlet cooling water was decreased with the same mass flow rate. But the uniformity of velocity field was improved, which increased the mean temperature difference between cooling water and battery surface. As a result, both the maximum temperature and maximum temperature difference decreased. The Table 3 shows that as the space increased the pressure drop decreased obviously, which led to less energy consumption. When the space was 6mm, the pressure drop was under 5 Pa. And the pressure drop decreased 96% as space between adjacent batteries was changed from 3 mm to 8 mm.

Table 3 Pressure drop under different space between adjacent batteries

Space (mm)	3	4	5	6	7	8
Pressure drop (Pa)	42.3	15.75	7.35	3.45	2.55	1.65

Larger space between adjacent batteries could decrease the energy density of pack but lead to lower temperature and pressure drop. Fig. 4 (b) shows the PCM exceeded melting point closed to the battery with different space between adjacent batteries. It can be seen that the volume fraction of PCM exceeded melting point decreased as the space between adjacent batteries increased as a result of more heat being moved by cooling water.

3.3 Effect of cooling water mass flow rate
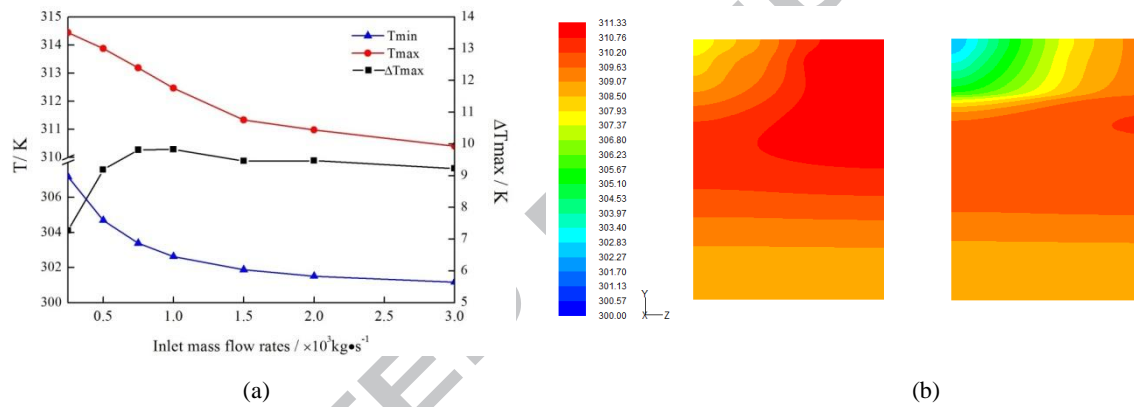
(a)   (b)

Fig. 5. (a) Temperature of the module under different inlet mass flow rates. (b) Temperature distribution of battery (center section on the left, surface on the right), at the end of the discharging, $H = 5$ cm, $L = 4$ mm $Q = 0.0015$ kgs^{-1}.

In the module with PCM/water-cooling plate, the mass flow rate of cooling water is an important factor. In this section, eight types of inlet mass flow rate, which changed from 0.25×10^{-3} kg·s^{-1} to 3×10^{-3} kg·s^{-1} and a 5 cm cooling-plate was chosen to study its influence on cooling performance. The maximum temperature and minimum temperature is shown in Fig.5 (a), as well as the maximum temperature difference. It indicates that the maximum temperature and minimum temperature of the pack decreased 4.04 K and 6 K, respectively, as the mass flow rate changed from 0.25×10^{-3} kg·s^{-1} to 3×10^{-3} kg·s^{-1}. When inlet mass flow rate was higher than 1×10^{-3} kg·s^{-1}, the maximum temperature was under 313 K (40 ℃) at the end of 2 C discharging, which was upper optimum working temperature. The higher the inlet mass flow rate was, the more maximum temperature decreased. However, the

downtrend of maximum temperature decreased with the increase of inlet mass flow rate. The maximum temperature difference increased 9.83 K then decreased slowly. It indicates that it is very difficult to reduce the maximum temperature difference in the pack down to 5 K. As the velocity of cooling water increased, the heat transfer rate between cooling water and battery increased obviously. And the temperature rising of cooling water was reduced during the progress of heat transfer, which increased the mean temperature difference between the battery and the cooling water. The increasing of the heat transfer rate and mean temperature difference improved the cooling performance. As the mass flow rate of cooling water increased, the maximum temperature difference exceeded 5 K at 965 s, 771 s, 681 s, 641 s, 612 s, 614 s and 650 s respectively during the 2 C discharging progress. The temperature distribution of battery with maximum temperature in the module at the end of the discharging was shown in Fig.5 (b). The minimum temperature appeared at the battery surface close to the cooling water inlet. And the maximum temperature appeared at the center section close to the negative electrode, where the heat generation was high. As it is shown in the Fig.6, the velocity of cooling water near the negative electrode was small, which decreased the cooling performance and increased the maximum temperature difference. It was hard to control the maximum temperature difference less than 5 K.
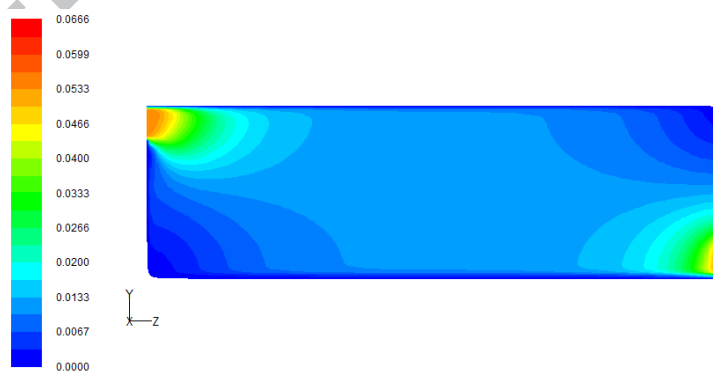
Fig. 6. Velocity distribution of cooling water, H = 5cm, L = 4mm Q = 0.0015 $kg \cdot s^{-1}$.

Pressure drops under different mass flow rate are shown in Table 4. When mass flow rate was changed from 0.25×10^{-3} $kg \cdot s^{-1}$ to 3×10^{-3} $kg \cdot s^{-1}$, the pressure drop increased quickly. That is because the velocity of cooling water in cooling plate decreased, which increased the on-way resistance and local resistance.

Table 4 Pressure drop under different inlet mass flow rate

Mass late rate ($\times 10^3$ kg·s^{-1})	0.25	0.5	0.75	1.0	1.5	2.0	3.0
Pressure drop (Pa)	3.9	7.8	11.7	15.75	23.7	31.95	48.6

Higher mass flow rate will cause higher pressure drop but better temperature field. It is necessary to choose

appropriate mass flow rate to keep the balance of energy consumption and cooling performance.

3.4 Effect of flow direction

The temperature near the electrode of the pouch battery is highest during the discharging. Compared to the

temperature of negative electrode area, temperature of positive electrode area is higher. Flow direction of cooling

water affects the temperature and its distribution. In this section, 6 cases with different flow directions were

considered and simulated. The inlet mass flow rate is 1×10^{-3} kg·s^{-1}, and the height of cooling plate is 5 cm. In the 6

cases, the setting of water inlets and outlets in adjacent cooling plate was different, as it was shown in Fig. 7.
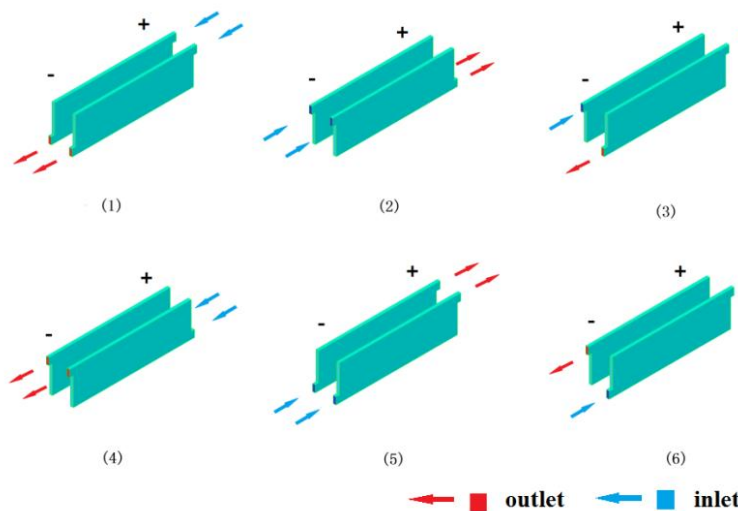
Fig.7. Design of different flow direction
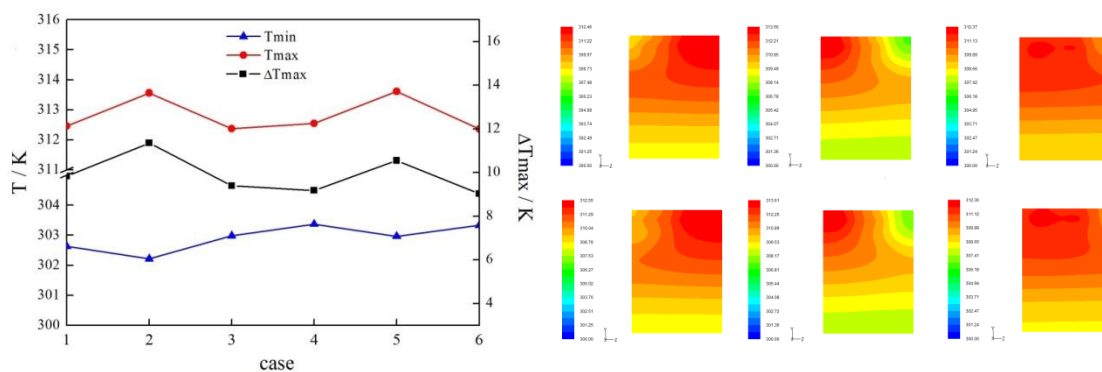
(a)   (b)
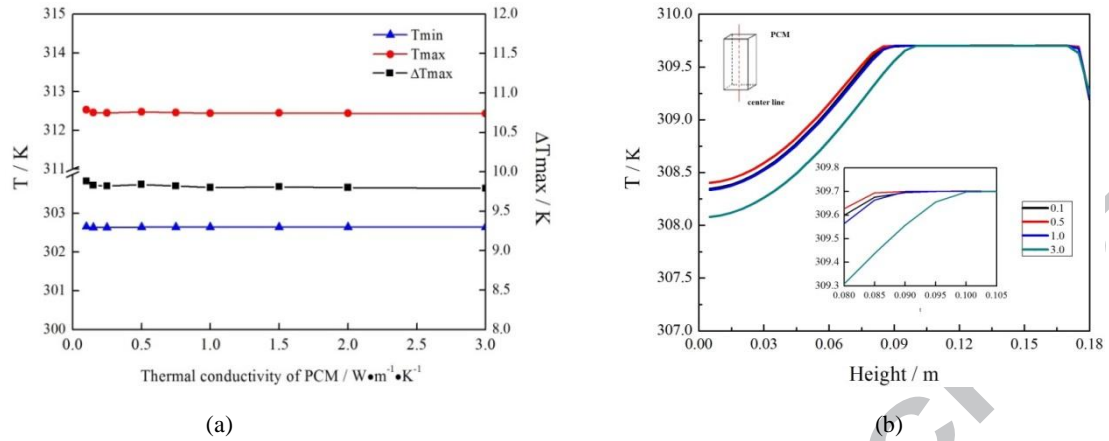
Fig. 8. (a) Temperature of the module under different flow direction. (b) Temperature distribution of battery center section with

different flow direction (case 1, case 2, case 3, case 4, case 5, case 6) at the end of the discharging.

The maximum temperature and minimum temperature versus different cases were shown in Fig.8 (a), as well as

the maximum temperature difference. Comparing the maximum temperature and maximum temperature difference

of case 1 with case 3, it can be seen that inlet of cooling water on different sides made a better cooling performance.

In the case 1, the velocity of cooling water close to the positive electrode area was bigger than that close to the

negative electrode area, as it is shown in the Fig.6. The velocity difference made the difference of heat transfer rate,

which affected the cooling performance of high generation area. Cooling water flowing into the gaps between

adjacent batteries from different sides could decrease the heat transfer rate difference, which made lower maximum

temperature and maximum temperature difference. Temperature distribution of battery in center section is shown in

the Fig.8 (b). The maximum temperature had little difference between case 1 and case 2, which was the same

between case 4 and case 5. It indicates that inlet on positive side or negative side made no obvious difference.

Comparing case 3 with case 6 and comparing case 1 with case 4, it shows that setting higher inlet mad no obvious

difference in maximum temperature but leaded to higher minimum temperature, which decreased the maximum

temperature difference as a result.

Cooling water flowing into the gap between adjacent batteries with different direction made the heat transfer rate

higher and more uniform in high generation area. The temperature uniformity was improved, which had a positive

effect on safety and life of batteries. And the higher inlet can leaded to larger mean temperature difference.

3.5 Effect of thermal conductivity and melting point of PCM

(a)   (b)

Fig. 9. (a) Temperature of the module under different thermal conductivity of PCM. (b) Temperature of PCM along the center line under different thermal conductivity of PCM

Fig. 9 (a) displays the maximum temperature, minimum temperature and maximum temperature difference of module with different thermal conductivity of PCM. The increase of the thermal conductivity leads to the slow decrease of the maximum temperature of the battery at the end of the discharging. However, the maximum temperature difference was almost constant, as the region with minimum temperature was close to the water cooling plate. The heat was absorbed as latent heat by the PCM because of the large heat storage capacity of PCM. The variation trend of maximum temperature difference is the same with that of maximum temperature. And the temperature of the PCM did not exceed the melting point at the end of 2 C discharging, as the thermal conductivity increased from $0.1 \, W \cdot m^{-1} \cdot K^{-1}$ to $3 \, W \cdot m^{-1} \cdot K^{-1}$. The Fig.9 (b) shows the temperature profile along the center line of PCM close to the battery with different PCM thermal conductivity at the end of 2 C discharging. It can be seen that the temperature of the PCM could not exceed the melting point. When the thermal conductivity of PCM was 0.5 $W \cdot m^{-1} \cdot K^{-1}$, the PCM above 0.085 m began to melt. It shown that the rate of melting PCM decreased as the thermal conductivity increased.

As the thermal conductivity has small influence on the cooling performance in this system, there is no need to increase the thermal conductivity of PCM by foam metal or high thermal conductive additive, which increases the weight but decrease the latent heat of PCM.
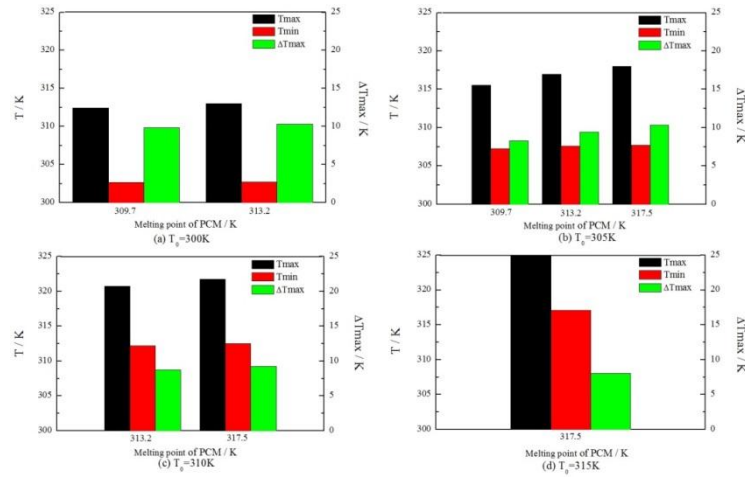
20

Fig. 10. Temperature of the module with different melting point of PCM under different environment temperature.

In order to research the effect of PCM melting point on the module under different environment temperature, we chose four kinds of PCM with different melting point as the environment temperature changed from 300 K to 315 K and the melting point of PCM was higher than the environment temperature. The temperature of cooling water and initial temperature of module were equal to the environment temperature. The simulated result was shown in Fig. 10. When the melting point of PCM increased but the environment temperature was constant, the maximum temperature and the maximum temperature difference of module both increased. When the melting point of PCM was constant and the environment temperature increased, the maximum temperature of module increased and the maximum temperature difference decreased. The uniformity of temperature field was improved.

In order to improve the environmental suitability of module, increasing the melting point of PCM and decreasing the temperature of inlet cooling water properly was necessary.

3.6 Performance of preventing of thermal runaway
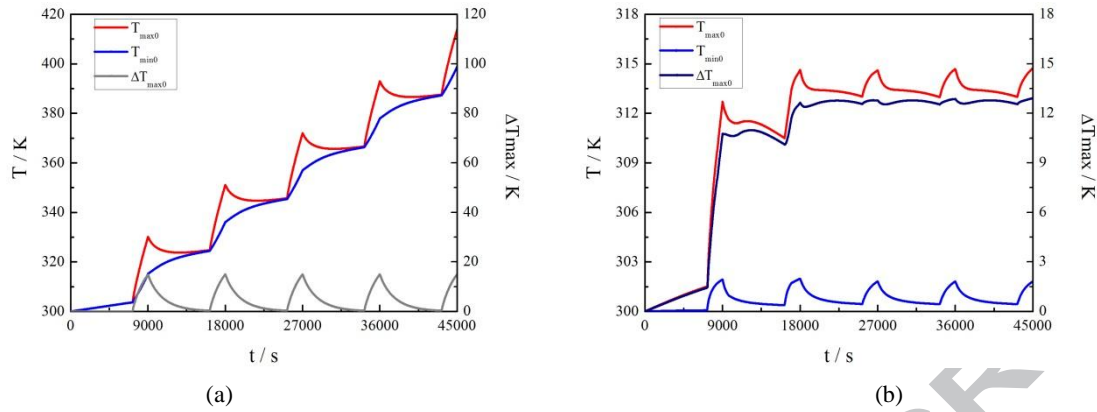
(a)   (b)

Fig. 11. (a) Temperature of module without PCM/water cooling plate after 5 continuous charge-discharge cycles. (b) Temperature of module with PCM/water cooling plate after 5 continuous charge-discharge cycles.

Continuous charge-discharge cycles would result in high temperature of module and even lead to thermal runaway, which was dangerous. We simulated the effect of PCM/water cooling plate on temperature controlling of module after 5 continuous charge-discharge cycles. Each charge-discharge cycles sustained 9000 s and consisted of a 0.5 C charging progress and a 2C discharging progress. The environment temperature was 300 K and the melting point of PCM was 313.2 K. Fig. 11 shown the temperature conditions of module without PCM/water cooling plate and module with PCM/water cooling plate after 5 continuous charge-discharge cycles.

It shown that the maximum temperature of module without PCM/water cooling plate after 5 charge-discharge cycles exceeded 410 K, which would lead to liquation of membrane [29]. When the membrane liquated, the internal short-circuit would happen and the temperature rose further, which would lead to the thermal runaway of battery [30]. With the PCM/water cooling plate, the maximum temperature of module exceeded 310 K after first charge-discharge cycle. Compared with 2 C discharging progress, the heat generation of each region during 0.5 C charging progress was relatively balance. The maximum temperature of module decreased during the second charging progress as some heat was conducted from near-electrode area to low temperature region. After 2 continuous charge-discharge cycles the maximum temperature reached peak and changed periodically in the subsequent 3 cycles. And in this progress the latent heat of PCM came into play. In addition, the maximum

22

temperature difference of module with PCM/water cooling plate staid at 13 K. While the maximum temperature difference of module without PCM/water cooling plate staid at 13K kept rising during all the 5 cycles.

PCM/water cooling plate could limit the maximum temperature effectively and improve the uniformity of temperature field during the 5 continuous charge-discharge cycles. As a result, it prevented the emergence of thermal runaway and increased the safety of module.

4 Conclusion

The PCM and water cooling plate were coupled together to improve the working performance of the lithium ion battery module as the liquid could lead to the desirable cooling performance and PCM could improve the temperature uniformity. The lithium-ion battery module with PCM/water cooling-plate was designed and numerically analyzed based on the energy conservation and fluid dynamics. A 2-D internal heat source got from the electro-thermal coupled model for pouch battery LiFePO4/C battery was used in the numerical model. Factors such as height of water cooling-plate, space between adjacent batteries, inlet mass flow rate, flow direction, thermal conductivity and melting point of PCM were discussed to research their influences on the temperature field of module, pressure drops of cooling water. And the 5 continuous charge-discharge cycles was used to research the effect of PCM/water cooling plate on preventing thermal runaway. The numerical results are included:

(1) The PCM/water cooling plate provided good cooling efficiency in controlling the lithium-ion battery module temperature. And the 5 cm high cooling plate made the best cooling performance. As the space between adjacent batteries increased, the maximum temperature shown little change but the temperature field got more uniform.

(2) Increasing inlet mass flow rate could reduce the maximum temperature and was more efficient than other methods. But the energy consumption was higher as the pressure drop rose quickly. The energy consumption could be reduced by increasing the space between adjacent batteries or the height of cooling plate. Higher inlet of cooling

23

water would contribute to better cooling performance on high heat generation area, compared to that of high outlet.

(3) As the thermal conductivity has small influence on the cooling performance in this system, there is no need to increase the thermal conductivity of PCM by foam metal or high thermal conductive additive. In order to improve the environmental suitability of module, increasing the melting point of PCM and decreasing the temperature of inlet cooling water properly was necessary.

(4) The PCM/water cooling plate could limit the maximum temperature effectively and improve the uniformity of temperature field during the 5 continuous charge-discharge cycles. As a result, it prevented the emergence of thermal runaway and increased the safety of module.

Acknowledge

References

[1] A Greco, X Jiang, D.P Cao. An investigation of lithium-ion battery thermal management using paraffin/porous-graphite-matrix composite, J. Power Sources 278 (2015) 50–68.

[2] H. Park, A design of air flow configuration for cooling lithium ion battery in hybrid electric vehicles, J. Power Sources 239 (2013) 30-36.

[3] D.F Chen, J.C Jiang, G Kim, C.B Yang, Ahmad Pesaran. Comparison of different cooling methods for lithium ion battery cells, Appl Therm Eng 94 (2016) 846–854.

[4] M Fleckenstein, O Bohlen, MA. Roscher, B Baker. Current density and state of charge inhomogeneities in Li-ion battery cells with LiFePO4 as cathode material due to temperature gradients, J. Power Sources 196 (2011) 4769–4778

[5] TH Tran, S Harmand, B Sahut. Experimental investigation on heat pipe cooling for Hybrid Electric Vehicle and Electric Vehicle lithium-ion battery, J. Power Sources 265 (2014) 262-272

[6] Q Wang, B Jiang, B Li, et al. A critical review of thermal management models and solutions of lithium-ion batteries for the development of pure electric vehicles, Renewable & Sustainable Energy Reviews 64 (2016) 106-128.

[7] S Al-Hallaj, JR Selman. A novel thermal management system for EV batteries using phase change material (PCM), J. Electrochem Soc 147 (2000) 3231–3236.

[8] S Al Hallaj, J Selman. Thermal modeling of secondary lithium batteries for electric vehicle/hybrid electric vehicle applications, J. Power Sources 2002; 110:341–349.

[9] N Javani, I Dincer, GF Naterer, GL Rohrauer. Modeling of passive thermal management for electric vehicle battery packs with PCM between cells, Appl Therm Eng 73 (2014) 307-316.

[10] R Kizilel, R Sabbah, JR Selman, S Al-Hallaj. An alternative cooling system to enhance the safety of Li-ion battery packs, J. Power Sources 194 (2009) 1105–12.

[11] W.Q Li, Z.G Qu, Y.L He, W.Q Tao. Experimental and numerical studies on melting phase change heat transfer in open-cell metallic foams filled with paraffin, Appl Therm Eng 37 (2012) 1–9.

[12] EBS Mettawee, GMR Assassa. Thermal conductivity enhancement in a latent heat storage system, Sol Energy 81 (2007) 839–45.

[13] Y.F Lv,   X.Q Yang, X.X Li, Guoqing Zhang, Ziyuan Wang, Chengzhao Yang. Experimental study on a novel battery thermal management technology based on low density polyethylene-enhanced composite phase change materials coupled with low fins, Appl Energ, 178 (2016) 376–382.

[14] W.Q Li, Z.G Qu, Y.L He, W.Q Tao. Experimental study of a passive thermal management system for high-powered lithium ion batteries using porous metal foam saturated with phase change materials, J. Power Sources 255 (2014) 9-15.

[15] Z Rao, S Wang, G Zhang. Simulation and experiment of thermal energy management with phase change material for ageing LiFePO 4 power battery, Energ Convers Manage 52 (2011) 3408–3414.

[16] A Greco, D Cao, X Jiang, H Yang. A theoretical and computational study of lithium-ion battery thermal management for electric vehicles using heat pipes, J. Power Sources 257 (2014) 344–355.

[17] P Nelson, D Dees, K Amine. Modeling thermal management of lithium-ion PNGV batteries, J. Power Sources 110 (2002) 349–356.

[18] D Chen, J Jiang, G-H Kim, C Yang, A Pesaran. Comparison of different cooling methods for lithium ion battery cells, Appl Therm Eng 94 (2016) 846–54.

[19] J Zhao, Z Rao, Y Li. Thermal performance of mini-channel liquid cooled cylinder based battery thermal management for cylindrical lithium-ion power battery, Energ Convers Manage 103 (2015) 157–165.

[20] L Jin, P Lee, X Kong, Y Fan, S Chou. Ultra-thin mini-channel LCP for EV battery thermal management, Appl Energ 113 (2014) 1786–1794.

[21] Y Huo, Z Rao, X Liu, J Zhao. Investigation of power battery thermal management by using mini-channel cold plate, Energ Convers Manage 89 (2015) 387–395.

[22] S Panchal, R Khasow, I Dincer, M Agelin-Chaab, R Fraser, M Fowle. Thermal design and simulation of mini-channel cold plate for water cooled large sized prismatic Lithium-ion battery, Appl Therm Eng 122 (2017) 80-90.

[23] Z Qian, Y Li, Z Rao. Thermal performance of lithium-ion battery thermal management system by using mini-channel cooling, Energ Convers Manage 126 (2016) 622–631.

[24] S Panchal, I Dincer, M Agelin-Chaab, R Fraser, M. Fowler. Experimental and theoretical investigations of heat generation rates for a water cooled LiFePO4 battery, Int J Heat Mass Tran 101 (2016) 1093–1102

[25] R Liu, J Chen, J Xun, K Jiao, Q Du. Numerical investigation of thermal behaviors in lithium-ion battery stack discharge, Appl Energ 132 (2014) 288–297.

[26] Z Rao, Q Wang, C Huang. Investigation of the thermal performance of phase change material/mini-channel coupled battery thermal management system, Appl Energ 164 (2016) 659–669.

[27] S Tiari, S Qiu, M Mahdavi. Numerical study of finned heat pipe-assisted thermal energy storage system with high temperature phase change material, Energ Convers Manage 89 (2015) 833–42.

[28] M Chen, F Bai, W Song, J Lv, S Lin, Z Feng, Y Li, Y Ding. A multilayer electro-thermal model of pouch battery during normal discharge and internal short circuit process, Appl Therm Eng 120 (2017) 506-516.

[29] Q Wang, P Ping, X Zhao, G Chu, J Sun, C Chen. Thermal runaway caused fire and explosion of lithium ion battery, J. Power Sources 108 (2012) 210–224.

[30] Q Wang, P Ping, J Sun, C Chen. Cresyl diphenyl phosphate effect on the thermal stabilities and electrochemical performances of electrodes in lithium ion battery, J. Power Sources 196 (2011) 5960-5965.

Table captions

Table 1 Physical sizes and parameters used in simulation

Table 2 Pressure drop under different cooling plate height

Table 3 Pressure drop under different space between adjacent batteries

Table 4 Pressure drop under different inlet mass flow rate

Figure captions

Fig. 1. Schematic of lithium-ion battery module with PCM/water cooling-plate

Fig. 2. Simulated temperature cloud of pouch battery at the end of 2 C discharging

Fig. 3. (a) Temperature of the module under different cooling plate height. (b) Temperature of cell and PCM along the center line with different cooling plate height

Fig. 4. (a) Temperature of the module under different space between adjacent batteries. (b) The PCM exceeded melting point closed to the battery with different space between adjacent batteries (4 mm, 6 mm, 8 mm)

Fig. 5. (a) Temperature of the module under different inlet mass flow rates. (b) Temperature distribution of battery (center section on the left, surface on the right), at the end of the discharging, $H = 5$ cm, $L = 4$ mm $Q = 0.0015$ kgs^{-1}.

Fig. 6. Velocity distribution of cooling water, $H = 5$cm, $L = 4$mm $Q = 0.0015$ kg·s^{-1}.

Fig.7. Design of different flow direction

Fig. 8. (a) Temperature of the module under different flow direction. (b) Temperature distribution of battery center section with different flow direction (case 1, case 2, case 3, case 4, case 5, case 6) at the end of the discharging.

Fig. 9. (a) Temperature of the module under different thermal conductivity of PCM. (b) Temperature of PCM along the center line under different thermal conductivity of PCM

Fig. 10. Temperature of the module with different melting point of PCM under different environment temperature.

Fig. 11. (a) Temperature of module without PCM/water cooling plate after 5 continuous charge-discharge cycles. (b) Temperature of module with PCM/water cooling plate after 5 continuous charge-discharge cycles.

Highlight:

The lithium battery module with Phase change material/water cooling-plate was proposed.

The non-uniform internal heat source based on 2D electro-thermal model for battery LiFePO4/C was used.

The water cooling-plate can cool the high heat generation area of battery effectively.

The Phase change material /water cooling plate can prevent the thermal runaway at the end of 5 continuous charge-discharge cycles.